

Balance Control of Brushless Direct Current Motor Driven Two-Rotor UAV

Ibrahim Cukdar ¹, Tevfik Yigit ^{2,*} and Hakan Celik ¹

¹ Department of Mechatronics Engineering, Faculty of Engineering, Firat University, 23119 Elazığ, Turkey; ibrahimcukdar41@gmail.com (I.C.); hakancelik@firat.edu.tr (H.C.)

² Department of Mechatronics Engineering, Faculty of Engineering, Nigde Ömer Halisdemir University, 51240 Nigde, Turkey

* Correspondence: tevfikyigit@ohu.edu.tr

Abstract: In this study, the balance control of a Brushless Direct Current Motor (BLDCM) driven Two-Rotor UAV (2R-UAV) was carried out. First, a MATLAB/Simulink model of the balance system of the 2R-UAV was built. Afterwards, classical and 2-DOF PID, and proposed Adaptive Fuzzy (AF) 2-DOF PID control structures were created on the STM32F4 microprocessor for both balance angle of the system and speed control of the BLDCMs. Classical and 2-DOF PID controller parameters were determined via Particle Swarm Optimization (PSO), a technique that is commonly used in control applications. For the balance control of the 2R-UAV, a Co-Simulation structure was created using the STM32F4 microprocessor and MATLAB/Simulink, and the performances of classical and 2-DOF PID, and AF 2-DOF PID controllers were examined comparatively. Upon examining the comparison results, it was found that the classical and 2-DOF PID, and AF 2-DOF PID stably controlled the balance of the 2R-UAV. The AF 2-DOF PID controller, proposed in this research, performed better than the classical and 2-DOF PID, especially under variable operating conditions.

Keywords: Two-Rotor UAV; Adaptive Fuzzy 2-DOF PID; BLDC Motor; Co-Simulation



Citation: Cukdar, I.; Yigit, T.; Celik, H. Balance Control of the Brushless Direct Current Motor Driven Two-Rotor UAV. *Appl. Sci.* **2024**, *14*, 4059. <https://doi.org/10.3390/app14104059>

Academic Editor: Rosario Pecora

Received: 9 April 2024

Revised: 30 April 2024

Accepted: 8 May 2024

Published: 10 May 2024



Copyright: © 2024 by the authors. Licensee MDPI, Basel, Switzerland. This article is an open access article distributed under the terms and conditions of the Creative Commons Attribution (CC BY) license (<https://creativecommons.org/licenses/by/4.0/>).

1. Introduction

In recent years, UAVs have been widely used in logistics, surveillance and warning systems, geographic information systems, fire extinguishing, and agricultural pest control [1–3]. The modeling of UAVs, with an ever-increasing scope of use, has recently been the subject of many scientific studies. The modeling enables the determination of the system reliability of UAVs and the study of their behaviour under different operating conditions. In the literature, the two-rotor balance system is also referred to as the Seesaw [4–6]. The two-rotor balance system is used primarily for the analysis of multi-rotor systems and is important as the basis of UAV systems [6]. Therefore, two-rotor systems are used for the study of the 2R-UAV balance System. The effectiveness of the control structure used determines how well two-rotor and multi-rotor UAVs operate [7]. Thus, research has been conducted to enhance the two-rotor system's balance control. An example of a 2R-UAV for load carrying operations is given in Figure 1.

Brushless Direct Current Motor (BLDCM) is one of the most preferred motor types in recent years due to its superior abilities, such as operating at high torque and speed, high efficiency, noiseless operation, long lifespan and minimal maintenance because brush and collector structures are not required [2,8]. It is commonly used in numerous industries, including aerospace, robotics, automotive, white goods, healthcare, and space, as a result of these outstanding qualities [2,9]. Thus, BLDCMs were used in this study to drive the 2R-UAV system.

In the literature, UAVs are typically controlled by classical PID and 2-DOF PID controllers, which have been successfully applied in control systems recently [3,10,11]. Additionally, artificial intelligence-based controller structures are also used to control UAVs [12–14].

In this study, unlike the control structures commonly used in the literature, an AF 2-DOF PID controller, which is a combination of 2-DOF PID and artificial intelligence and fuzzy logic control methods, was used for the 2R-UAV's balance control. The outcomes were compared with those of classical PID and 2-DOF PID controllers in order to assess the effectiveness of the AF 2-DOF PID controller. Also, in this study, differing from the studies in the literature, the speeds of the BLDCMs used as the drive elements, as well as the balance angle, were controlled in a closed loop, and the control performance of the balance angle was improved. Under identical settings, the parameters of the classical and 2-DOF PID controllers utilized in the study were determined using the Particle Swarm Optimization (PSO) technique, which has been commonly used to determine controller parameters in current research [2,15–17]. To examine the real-time performance of the controllers used in the study on a microprocessor, the Co-Simulation structure of the system was created using the STM32F4 microprocessor and MATLAB/Simulink. The performance of classical and 2-DOF PID, and AF 2-DOF PID controllers was comparatively examined using Co-Simulation results.

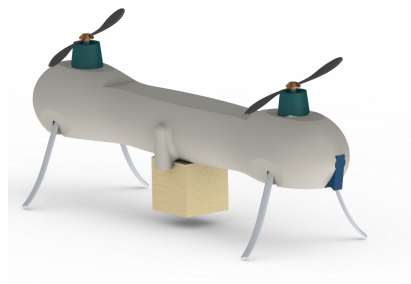


Figure 1. A 2-Rotor UAV example for load carrying operations.

Upon analysing the simulation results, we observed that the 2R-UAV balance system was steadily controlled by the classical PID, 2-DOF PID and suggested AF 2-DOF PID controllers. However, we observed that the AF 2-DOF PID controller that is suggested in this study showed a better performance than the other controllers used in the study, especially under variable operating conditions, demonstrating adaptive features.

The manuscript is structured as follows, in six different sections: in Section 2, the Simulink model of the BLDCM is presented, and detailed mathematical modeling is provided. In Section 3, the mathematical model and control structures of the 2R-UAV system are presented. In Section 4, the Co-Simulation structure and test setup of the 2R-UAV balance system are presented. Co-Simulation results of the 2R-UAV balance system according to different controllers are presented and discussed in Section 5. Finally, conclusions are clearly explained, and future works are provided in Section 6.

2. Brushless Direct Current Motor

The biggest advantage of Brushless DC Motors (BLDCMs) over traditional brushed DC motors is that they do not have brushes or collectors. In brushed DC motors, the component used to electrify the rotor's windings, which is the moving part, is called a "Brush", and the parts of the rotor on which the brushes touch are called "Collectors". In BLDCMs, the role of the brush and collector structure is replaced with an electronic controller, resulting in an electronically commutated direct current motor. Semiconductor circuit elements perform the current switching task in BLDCM drivers, while a microprocessor calculates the switching times. To avoid problems in the motor's rotation, the controller must accurately follow the rotor speed. For the controller to maintain the rotor at the desired speed, the rotor position must be precisely known. Hall Effect sensors are commonly used in most applications to detect the rotor position [18].

2.1. Mathematical Model of the BLDCM

Figure 2 shows the equivalent electrical circuit of the BLDCM. Three-phase electricity is used to power this equivalent circuit. Other waveforms, such as square waves, can be

applied in place of a sinusoidal source, provided that the peak voltage stays within the motor’s maximum voltage limit [19,20].

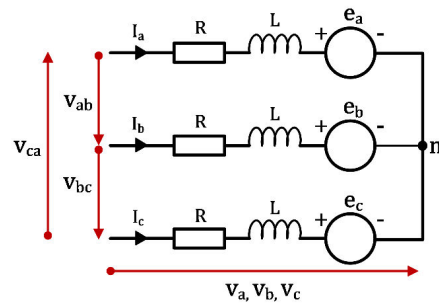


Figure 2. Electrical equivalent circuit of three-phase star-connected BLDCM.

Mathematical equations to be used in modeling can be obtained by using the electrical equivalent circuit of a star-connected three-phase BLDCM. Phase voltages are given in Equations (1)–(3).

$$v_a = R i_a + L \frac{d i_a}{dt} + e_a \tag{1}$$

$$v_b = R i_b + L \frac{d i_b}{dt} + e_b \tag{2}$$

$$v_c = R i_c + L \frac{d i_c}{dt} + e_c \tag{3}$$

Interphase voltages are given in Equations (4)–(6).

$$v_{ab} = R(i_a - i_b) + L \frac{d(i_a - i_b)}{dt} + e_a - e_b \tag{4}$$

$$v_{bc} = R(i_b - i_c) + L \frac{d(i_b - i_c)}{dt} + e_b - e_c \tag{5}$$

$$v_{ca} = R(i_c - i_a) + L \frac{d(i_c - i_a)}{dt} + e_c - e_a \tag{6}$$

Here, R is the stator phase resistance, L is the stator phase inductance, e_a , e_b and e_c are the back-EMF values, i_a , i_b and i_c are the phase currents that belongs to the winding stated in subscript, v_a , v_b and v_c are the phase voltages, and v_{ab} , v_{bc} and v_{ca} are the phase-to-phase voltages [2].

Equation (7) provides the phase current relationship.

$$i_a + i_b + i_c = 0 \tag{7}$$

If the interphase voltages are rearranged using Equation (7), the expressions given in Equations (8) and (9) are obtained. Thus, the voltage expressions between phases are reduced to two equations.

$$v_{ab} = R(i_a - i_b) + L \frac{d(i_a - i_b)}{dt} + e_a - e_b \tag{8}$$

$$v_{bc} = R(i_a + 2 i_b) + L \frac{d(i_a + 2 i_b)}{dt} + e_b - e_c \tag{9}$$

According to Newton’s second law of motion, the relationship between electromagnetic moment (T_e) and motor speed (ω_m) is given in Equation (10). The relationship between motor speed and mechanical angle (θ_m) is given in Equation (11).

$$T_e - T_L = J \frac{d \omega_m}{dt} + B \omega_m \tag{10}$$

$$\omega_m = \frac{d\theta_m}{dt} \tag{11}$$

Here, T_L is the load moment, J is the moment of inertia, B is the damping constant. The back-EMF expressions are given in Equations (12)–(14).

$$e_a = \frac{k_e}{2} \omega_m F(\theta_e) \tag{12}$$

$$e_b = \frac{k_e}{2} \omega_m F(\theta_e - \frac{2\pi}{3}) \tag{13}$$

$$e_c = \frac{k_e}{2} \omega_m F(\theta_e - \frac{4\pi}{3}) \tag{14}$$

The resulting total moment expression is given in Equation (15).

$$T_e = k_t [F(\theta_e)i_a + F(\theta_e - \frac{2\pi}{3})i_b + F(\theta_e - \frac{4\pi}{3})i_c] \tag{15}$$

Here, k_e and k_t are the back-EMF constant and the electromagnetic moment constant, respectively. The relationship between the electrical displacement (θ_e) and the rotor’s mechanical angle (θ_m) is given in Equation (16).

$$\theta_e = \frac{P}{2}\theta_m \tag{16}$$

Here, P is the number of poles of the motor. The function F , given in Equation (17), provides the back-EMF’s trapezoidal waveform based on the rotor position [21].

$$F(\theta_e) = \begin{cases} 1, & 0 \leq \theta_e \leq \frac{2\pi}{3} \\ 1 - \frac{6}{\pi}(\theta_e - \frac{2\pi}{3}), & \frac{2\pi}{3} \leq \theta_e \leq \pi \\ -1, & \pi \leq \theta_e \leq \frac{5\pi}{3} \\ -1 + \frac{6}{\pi}(\theta_e - \frac{5\pi}{3}), & \frac{5\pi}{3} \leq \theta_e \leq 2\pi \end{cases} \tag{17}$$

2.2. Matlab/Simulink Model of the BLDCM

The previously provided mathematical equations were used to model BLDCM in the Simulink environment. Following that, the Simulink model of the BLDCM and its drive system depicted in Figure 3 was built by incorporating the sub-models for the inverter and switching signals that are derived based on the data received from the Hall sensors.

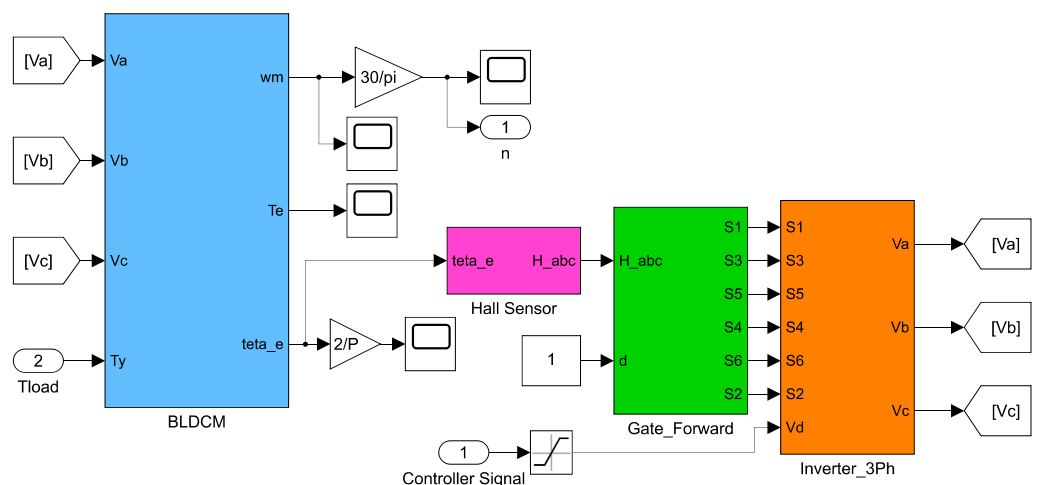


Figure 3. Model of the BLDCM drive system in Matlab/Simulink.

The parameters of BLDCM used in this study are given in Table 1.

Table 1. Parameters of the BLDCM.

Parameters	Values
R	0.304 Ω
L	0.2135 mH
P	16 Poles
B	0
V_d	24 V
J	181.10 ⁻⁷ kg·m ²
k_e	0.0369 V·s/rad
k_t	0.0369 Nm/A

3. Mathematical Model and Control of the Two-Rotor UAV System

Four or more rotor UAV systems are intricate and challenging to control. In order to control these systems, the dynamic behaviour of a simpler and unstable structure must be examined [22]. In this study, the 2R-UAV, which has a simpler structure than multi-rotor systems, was modeled in Simulink and its dynamic behaviour was examined. A SolidWorks drawing and a simplified diagram of the system are shown in Figure 4 [2].

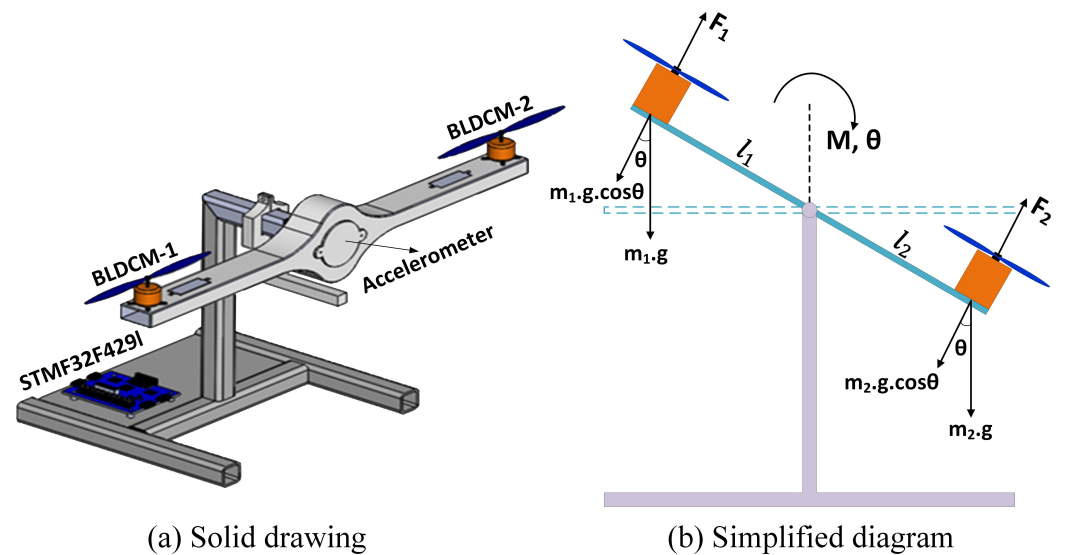


Figure 4. Two-Rotor UAV balance system.

Newton’s laws can be used to express the forces acting on the system when frictions are ignored, as shown in Figure 4. When the motors receive voltage in the 2R-UAV balance system, the propellers begin to rotate, producing a torque based on the values of the resulting F_1 and F_2 forces. The dynamic equations of the equilibrium system illustrated in Figure 4 are given by Equations (18) and (19), in accordance with Newton’s laws [2].

$$-l_1 m_1 g \cos(\theta) + l_2 m_2 g \cos(\theta) + l_1 F_1 - l_2 F_2 = -l_1^2 \ddot{\theta} m_1 - l_2^2 \ddot{\theta} m_2 \tag{18}$$

$$\ddot{\theta} = \frac{l_1 m_1 g \cos(\theta) - l_2 m_2 g \cos(\theta) - l_1 F_1 + l_2 F_2}{l_1^2 \ddot{\theta} m_1 + l_2^2 \ddot{\theta} m_2} \tag{19}$$

Here, $\ddot{\theta}$ is the angular acceleration. l_1 and l_2 represents the distance the arms are from the center to the motors, m_1 and m_2 represent the mass of the motors, and F_1 and F_2 represent the lifting forces. Using Equations (18) and (19), the Simulink model of the 2R-UAV balance system was built, as demonstrated in Figure 5.

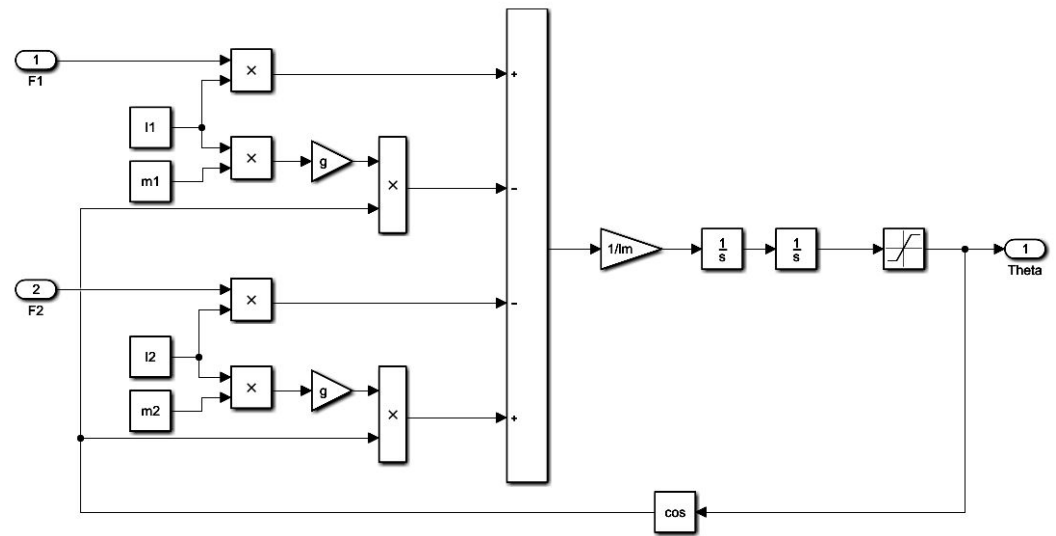


Figure 5. Model of the 2R-UAV balance system in Matlab/Simulink.

The parameters of the 2R-UAV balance system used in this study are provided in Table 2.

Table 2. Parameters of the 2R-UAV balance system.

Parameters	Values
Mass of the motor 1 (m_1)	$20 \cdot 10^{-3}$ kg
Length of the link 1 (l_1)	0.301 m
Mass of the motor 2 (m_2)	$20 \cdot 10^{-3}$ kg
Length of the link 2 (l_2)	0.301 m
Gravity (g)	9.81 m/s^2

3.1. Control of 2R-UAV Balance System Using Both Classical PID and 2-DOF PID Controllers

There is only one input (error) and one output (control signal) for a classical PID controller. As in all controllers, the purpose of the classical PID controller is to eliminate disturbing effects affecting the system and tracking the reference. To do this, the difference between the input and output is controlled [23]. Equation (20) provides the mathematical s-domain equation for the classical PID controller.

$$u(s) = [K_p + K_i s^{-1} + K_d s]e(s) \tag{20}$$

Here, $e(s)$ is the error signal used as input, $u(s)$ is the control signal used as output, K_p , K_i , and K_d respectively stand for the proportional, integral, and derivative terms.

There are a few benefits that the two-degree-of-freedom (2-DOF) controller offers over the single-degree-of-freedom (classical) controller. These benefits include lowering the impact of disruptive inputs and offering excellent performance in tracking the reference. The 2-DOF PID controller produces an output signal according to the difference within the actual value and the reference signal. Based on the stated weights of the proportional, integral, and derivative actions, it computes a weighted signal for each. The total of these actions on the corresponding difference signals, each of which is weighted in accordance with the chosen gain settings, is the controller output [24].

The mathematical s-domain equation of the 2-DOF PID controller is given in Equation (21).

$$u(s) = K_p(b r - y) + K_i s^{-1}(r - y) + K_d s(c r - y) \tag{21}$$

In this expression, $u(s)$ is the controller outcome, b is the proportional weight coefficient, c is the derivative weight coefficient, r is the reference input value and y is the system output. $K_{p,i,d}$ values have been employed in the classical PID expression.

Both the speed of the BLDCMs and the balance angle were controlled using classical and 2-DOF PID controllers. The parameters of these controllers were determined by the PSO. Figure 6 illustrates the Simulink model of the 2R-UAV system controlled by both classical and 2-DOF PID controllers.

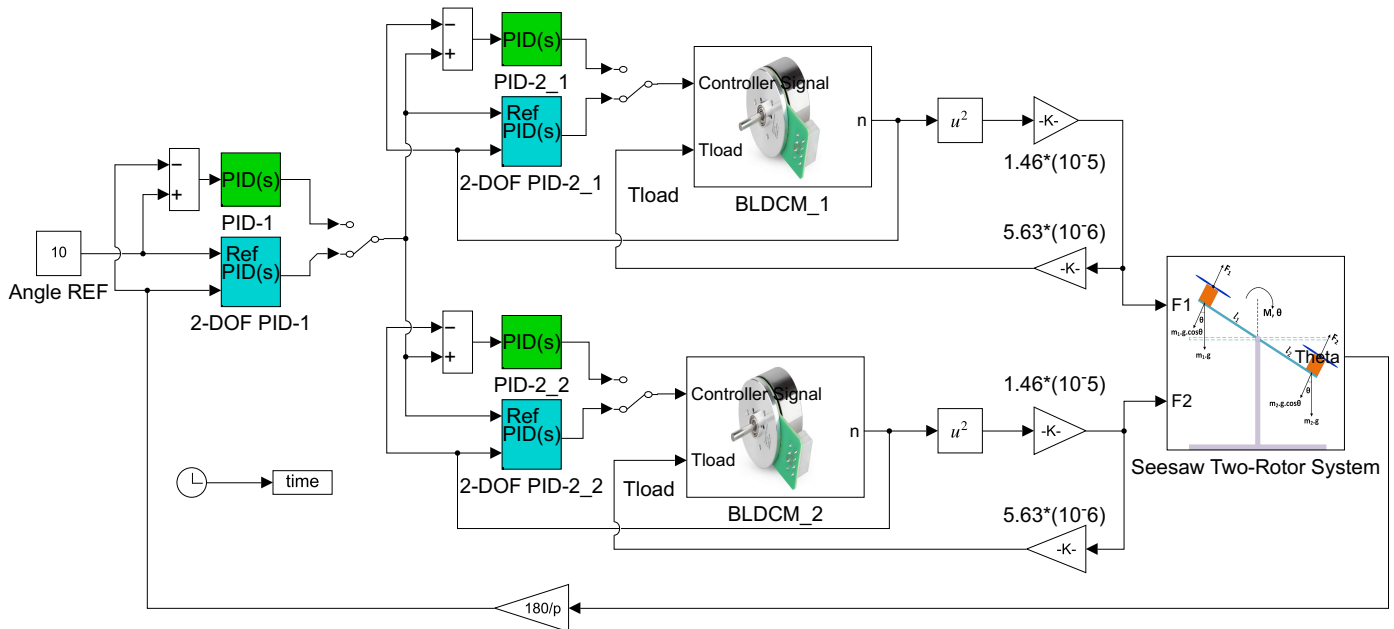


Figure 6. Classical and 2-DOF PID-controlled Matlab/Simulink model of the BLDCM driven 2R-UAV balance system.

As seen in Figure 6, the balance angle of the system changes with the effect of the F_1 and F_2 forces on the turning moment of the system, and the difference between this angle and the reference balance angle is entered into the controller. The output of this controller determines the speed difference of the motors. The reference speed of the BLDCM-1 is determined by adding the determined speed difference value to 2000 rpm, determined as the reference balance speed. Similarly, to determine the reference speed of the BLDCM-2, the speed difference value is subtracted from the 2000 rpm balance speed. Thus, closed-loop control of both balance angle and motor speeds is achieved. A pair of propellers called 1045 (10 × 4.5 inches), designed to produce thrust in clockwise and counter-clockwise rotations, are mounted to the motors. The F_1 and F_2 forces were determined by multiplying the square of the BLDCM-1 and BLDCM-2 motor speeds by the propeller thrust constant ($b = 1.46 \cdot 10^{-5} \text{ N s}^2$). By multiplying the F_1 and F_2 forces with the moment constant ($k = 5.63 \cdot 10^{-6} \text{ N m s}^2$), the load moments to be applied to the BLDCM-1 and BLDCM-2 motors were calculated.

Determining the Parameters of the Classical PID and 2-DOF PID Controllers Using the PSO

The controller parameters in this study were determined using PSO. It is an optimization algorithm discovered by Kennedy and Eberhart (1995) and created by taking advantage of the swarm behaviour, as in many optimization techniques [25]. All particles in the swarm try to move their position closer to the best position within the swarm, this process continues until the best position is reached [26,27]. All particles in the PSO algorithm are updated in each iteration with the best solution of the current iteration ($pbest$) and the best solution of all iterations ($gbest$) [26]. Expressions in which new particle velocities are determined are given in Equation (22), and new particle positions are given in Equation (23). Here, X_n and X_{n+1} are respectively the current and next positions of the particles, V_n and V_{n+1} are respectively the current and next speeds of the particles, c_1 and c_2 are the learning coefficients, and w is the inertia weight. $rand_1$ and $rand_2$ values are random numbers in the

range [0, 1], which can optionally be sampled from a uniform distribution. These random values add randomness to the optimization algorithm.

$$V_{n+1} = w V_n + c_1 rand_1(pbest_n - X_n) + c_2 rand_2(gbest_n - X_n) \tag{22}$$

$$X_{n+1} = X_n + V_{n+1} \tag{23}$$

Figure 7 shows the flow chart of the PSO algorithm.

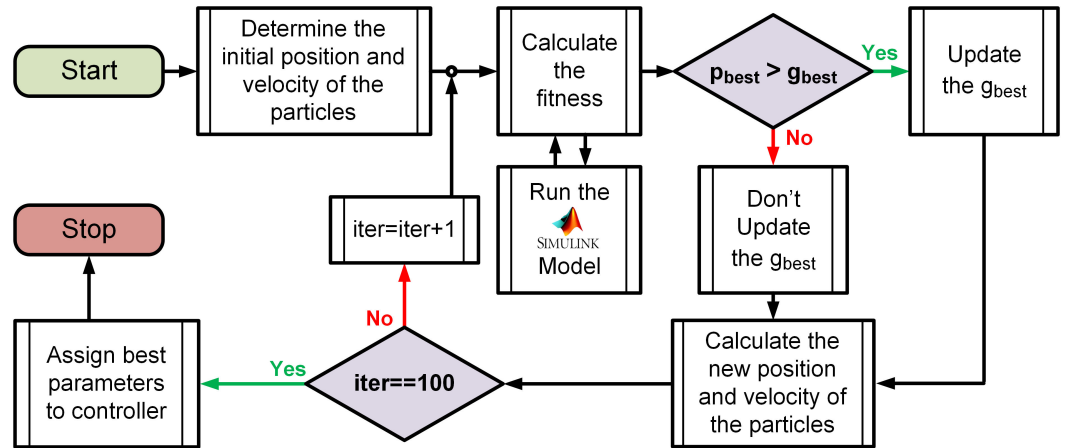


Figure 7. Flow chart of the PSO algorithm.

PSO parameters used to determine classical and 2-DOF PID controller optimization process are given in Table 3.

Table 3. PSO parameters used during optimizations.

Parameters	Classical PID	2-DOF PID
Number of individuals	100	100
Number of iterations	100	100
Number of parameters searched	6	10
Search space	$0 < (K_{p,i,d}) < 100$	$0 < (K_{p,i,d}) < 100$ $0 < (b, c) < 2$
w	0.9	0.9
c_1	0.12	0.12
c_2	1.2	1.2

The cost and PSO algorithms developed in Matlab were used to run the Simulink model shown in Figure 6 in order to find the controller parameters. The time-weighted integral of absolute error (ITAE), whose mathematical formula is provided in Equation (24), was utilized as the cost function when calculating the controller parameters with PSO.

$$J_{ITAE} = \int_0^{t_{simulation}} t |e(t)| dt \tag{24}$$

Here, J_{ITAE} is the optimization cost or performance index, as stated in the literature, t refers to time and $e(t)$ represents the error depending on time. Figure 8 illustrates the change in J_{ITAE} values during the optimization process used to determine the parameters of the controllers.

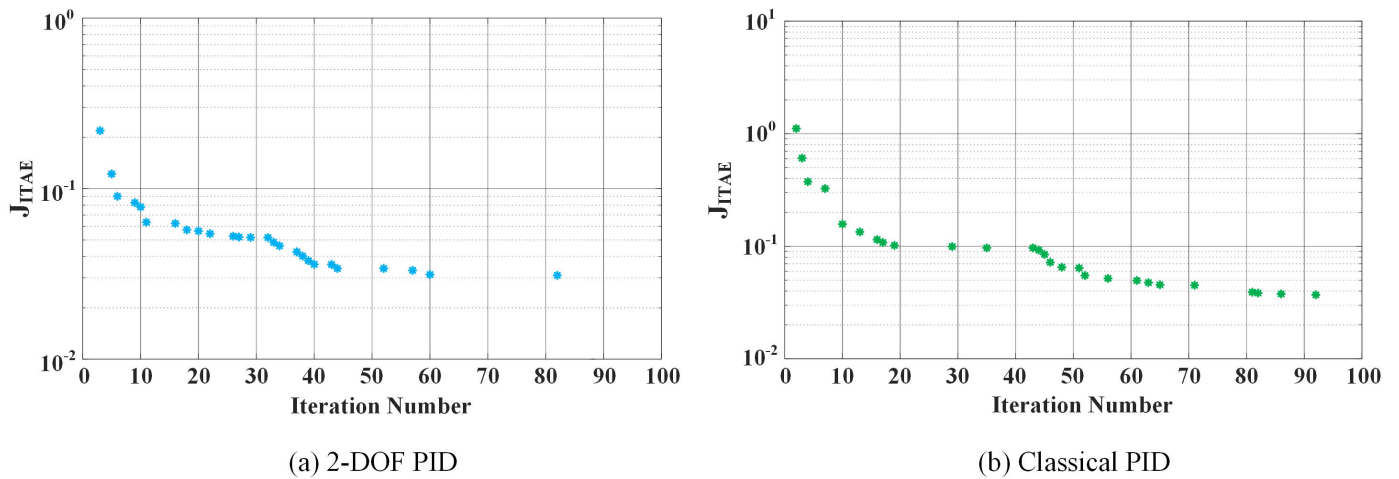


Figure 8. The change of the J_{ITAE} value during the optimization process.

The optimization-derived PID controller parameters are listed in Table 4.

Table 4. Classical PID controller parameters determined by PSO.

Balance System Angle Control		BLDCM Speed Control	
K_p	83.1974	K_p	56.6088
K_i	0.8507	K_i	53.6323
K_d	2.3771	K_d	0.0097

The optimization-derived 2-DOF PID controller parameters are listed in Table 5.

Table 5. 2-DOF PID controller parameters determined by PSO.

Balance System Angle Control		BLDCM Speed Control	
K_p	95.7409	K_p	64.4943
K_i	34.1622	K_i	8.8104
K_d	1.8018	K_d	0.0190
b	0.9914	b	1.0806
c	0.4508	c	0.9884

3.2. Control of 2R-UAV Balance System Using Offered Adaptive Fuzzy 2-DOF PID

In classical control systems, system’s mathematical model is created and controller used is built based on this model. In the fuzzy logic controller, the experience and control strategy of an expert opinion on the system are used as a database. While designing a fuzzy logic controller, in order to get the best efficiency from the controller, the expert who creates the control strategy must know the system very well [28]. The general structure of the fuzzy inference system is given in Figure 9 [29].

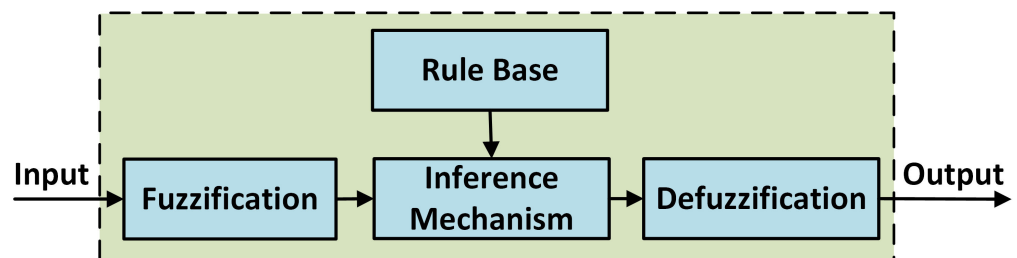


Figure 9. General structure of the fuzzy inference system.

In Figure 9:

- Fuzzification: Converts digital inputs into fuzzy data.
- Rule Base: Contains rule tables prepared by an expert opinion.
- Inference Mechanism: A fuzzy set is created for the output using membership functions and rule base.
- Defuzzification: Converts fuzzy data into digital outputs.

First, when designing a controller using fuzzy logic, input and output variables must be determined. Afterwards, the digital inputs of the fuzzy logic controller are converted into fuzzy data. A range is defined for specified inputs and outputs, and each is given a linguistic label. A membership function is created for each fuzzy subset given a linguistic label. Then, fuzzy inference is made using the fuzzy rule table created in the rule base. Fuzzy data generated by the application of fuzzy rules is converted into digital output by defuzzification [30].

The AF 2-DOF PID controller proposed in this study is a control method that combines fuzzy logic, an artificial intelligence control method, and a 2-DOF PID controller, one of the advanced control methods. In this fuzzy logic controller, normalized error (e) and change of error (Δe) are entered into the input of fuzzy logic. At the output of the fuzzy logic controller, K_p, K_i, K_d, b and c values are obtained as a result of the rule table determined by the input and output membership functions created. The 2-DOF PID parameters are determined by multiplying these values with the controller parameters previously determined by PSO.

Basis of the AF 2-DOF PID controller is given in Figure 10 [18].

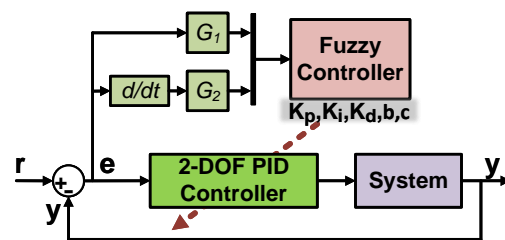


Figure 10. Basis of the Adaptive Fuzzy 2-DOF PID controller.

The Simulink model of the BLDCM driven 2R-UAV balance system with an AF 2-DOF PID controller is displayed in Figure 11. In this model, an AF 2-DOF PID controller is used for closed-loop control of both balance angle and BLDCM speeds.

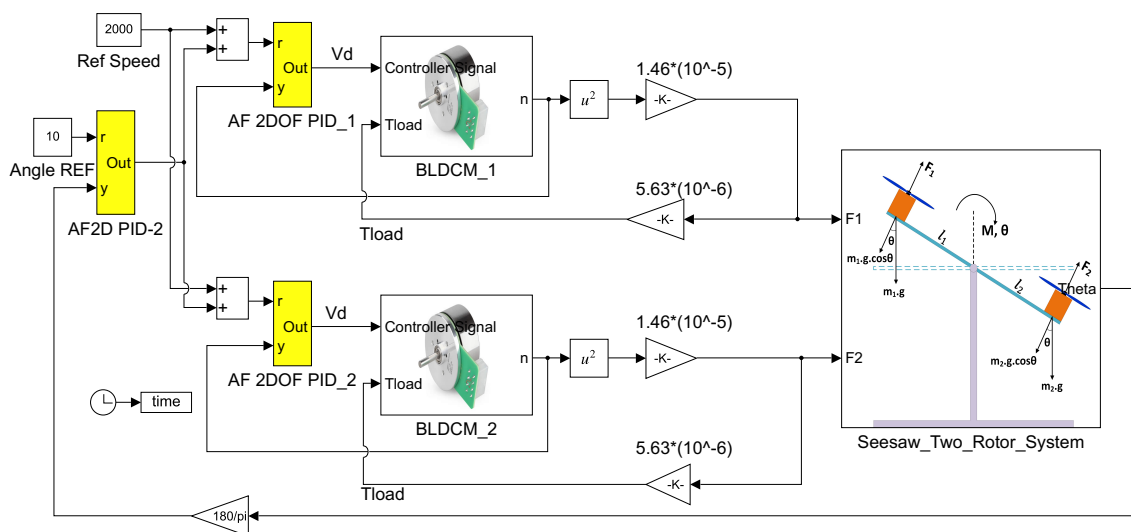


Figure 11. AF 2-DOF PID controlled Matlab/Simulink model of BLDCM driven 2R-UAV balance system.

Figure 12 shows the internal structure of the AF 2-DOF PID controller’s fuzzy logic controller block.

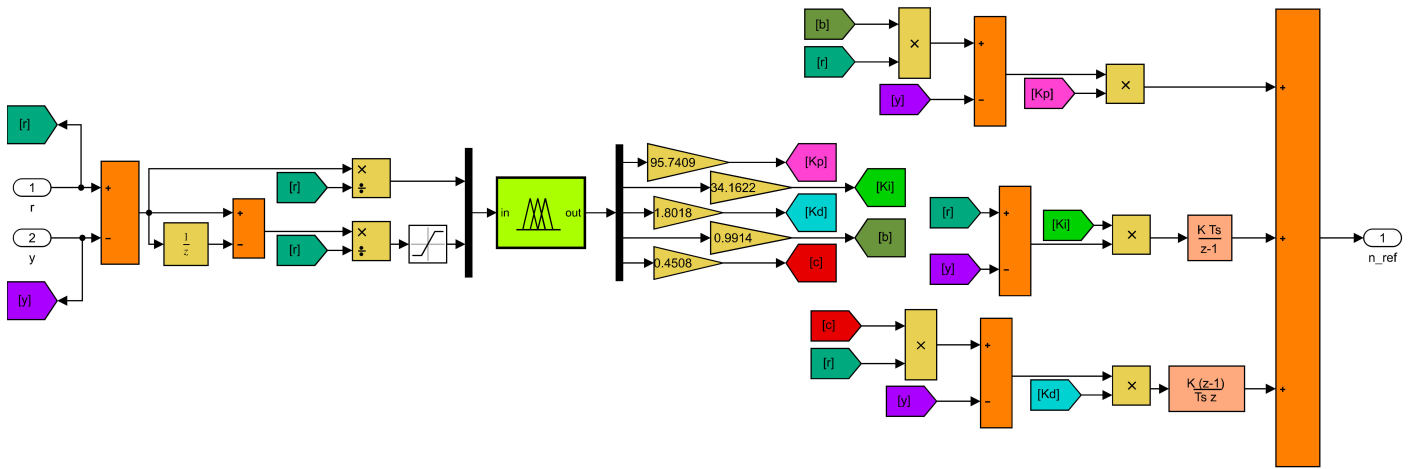


Figure 12. Adaptive Fuzzy 2-DOF PID controller block.

Fuzzy logic membership functions used to control both balance angle and BLDCM speeds in the system are given in Figures 13 and 14, and the rule tables are given in Tables 6 and 7.

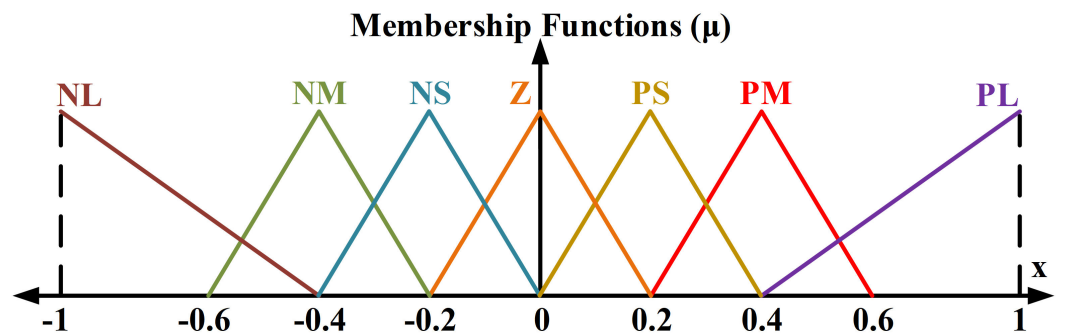


Figure 13. e and Δe input membership functions of balance angle and BLDCM speed controllers.

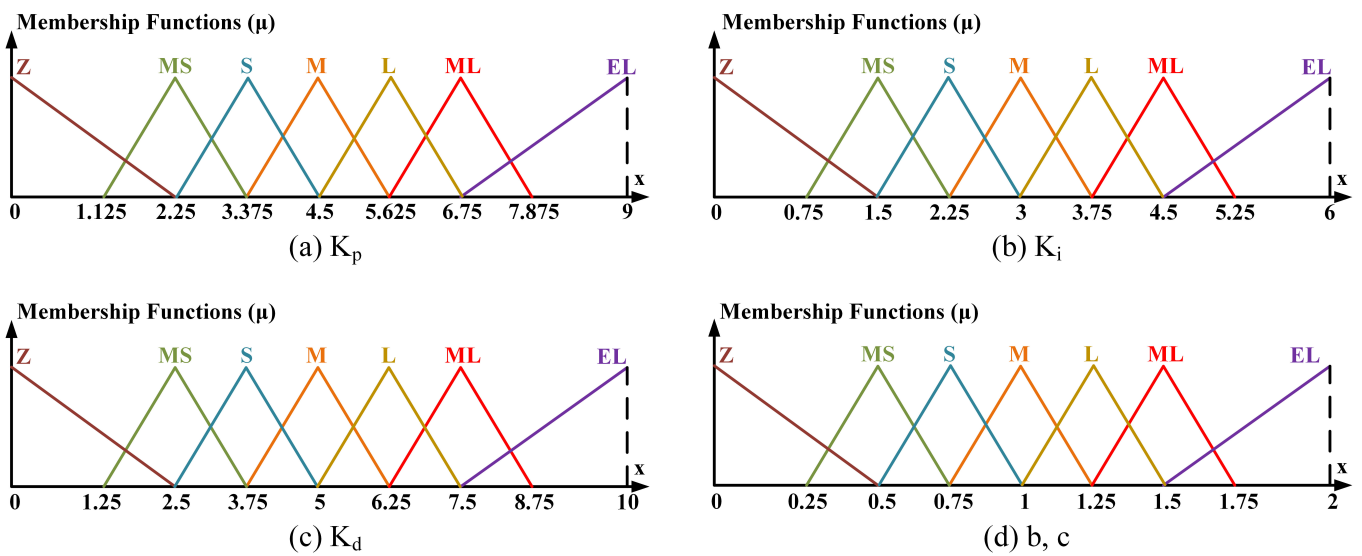


Figure 14. Output membership functions of the balance angle controller.

Table 6. Fuzzy logic rule table of BLDCM speed controller.

		$K_p/K_i/K_d/b/c$				
		Δe				
		NL	NS	Z	PS	PL
e	NL	ML/L/Z/S/Z	L/M/MS/MS/MS	MS/S/S/ML/S	L/M/M/MS/M	ML/L/ML/S/ML
	NS	ML/L/MS/S/MS	L/M/M/MS/M	S/S/L/M/L	L/M/ML/MS/ML	ML/L/ML/S/ML
	Z	ML/L/S/S/S	S/M/L/L/L	M/S/L/M/M	L/M/ML/M/ML	ML/L/ML/S/ML
	PS	ML/L/L/S/L	S/M/ML/L/ML	S/S/ML/ML/ML	ML/M/EL/MS/ML	ML/L/ML/S/ML
	PL	ML/EL/EL/Z/ML	M/M/EL/M/EL	S/S/EL/M/ML	ML/M/EL/S/ML	EL/L/EL/Z/ML

Table 7. Fuzzy logic rule table of the balance angle controller.

		$K_p/K_i/K_d/b/c$				
		Δe				
		NL	NS	Z	PS	PL
e	NL	ML/L/Z/MS/Z	L/M/MS/MS/MS	MS/MS/S/ML/S	L/M/M/S/M	ML/L/ML/MS/ML
	NS	ML/L/MS/MS/MS	L/M/M/S/M	M/M/L/M/L	L/M/ML/S/ML	ML/L/ML/MS/ML
	Z	ML/L/S/MS/S	S/M/L/L/L	M/S/L/M/L	M/M/ML/M/ML	ML/L/ML/MS/ML
	PS	ML/L/L/MS/L	S/M/ML/L/ML	MS/M/ML/ML/ML/M/EL/S/ML	ML/L/EL/MS/ML	ML/L/EL/MS/ML
	PL	EL/L/EL/Z/ML	M/M/EL/M/ML	M/S/EL/M/ML	ML/M/EL/MS/ML	EL/L/EL/Z/ML

The normalized error (e) and change of error (Δe) input variables of the balance angle and BLDCM speed controllers are expressed with seven triangular membership functions, as seen in Figure 13. These membership functions are named with the linguistic labels NL (negative large), NM (negative medium), NS (negative small), Z (zero), PS (positive small), PM (positive medium), PL (positive large).

The balance angle and K_p, K_i, K_d, b and c output variables of the BLDCM speed controller are expressed with seven triangular membership functions, as seen in Figures 14 and 15. These membership functions are named with the linguistic labels Z (zero), MS (middle-small), S (small), M (middle), L (large), ML (middle-large), EL (extra-large).

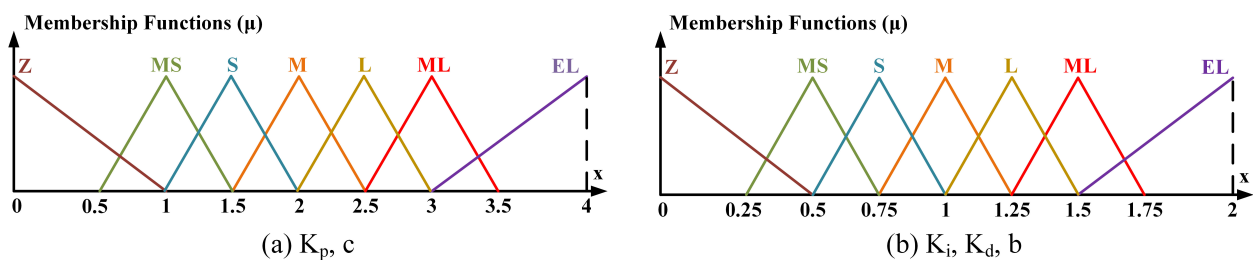


Figure 15. Output membership functions of the BLDCM speed controller.

4. Co-Simulation of BLDCM Driven Two-Rotor UAV Balance System

The STM32F429I discovery development board produced by ST Microelectronics, used in Co-Simulation studies, is widely used and easy to find. This is due to its low cost and its high performance based on ARM. Additionally, it is an important advantage that it can be programmed visually via Waijung block set on the Matlab/Simulink. This card aims to provide high performance with low power consumption [31]. Figure 16 shows the block diagram of the Co-Simulation system.

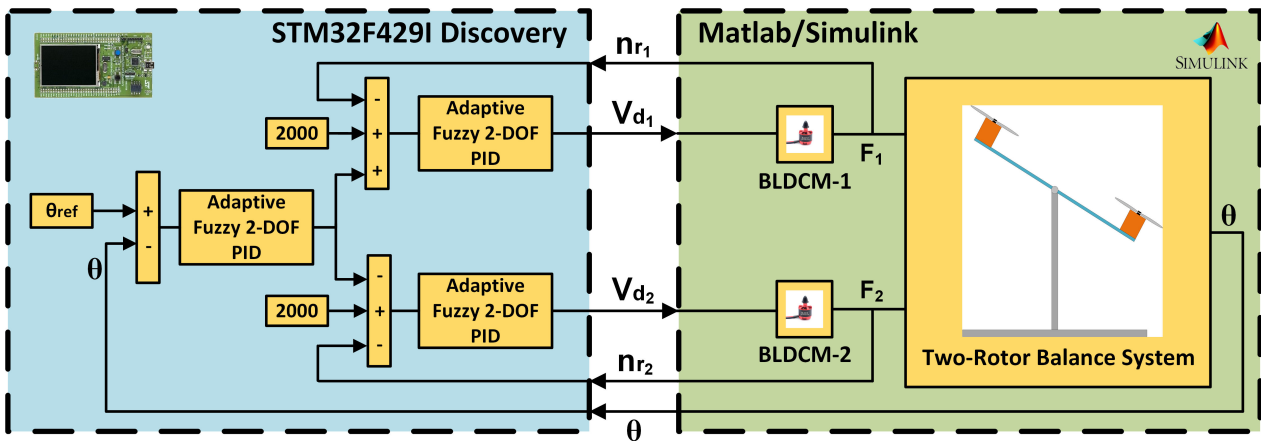


Figure 16. Block diagram of the Co-Simulation.

The simulation test setup created using with the Matlab/Simulink model and STM32F429I microprocessor (STMicroelectronics NV, Geneva, Switzerland) is given in Figure 17. Co-Simulation results were obtained from using this test setup.

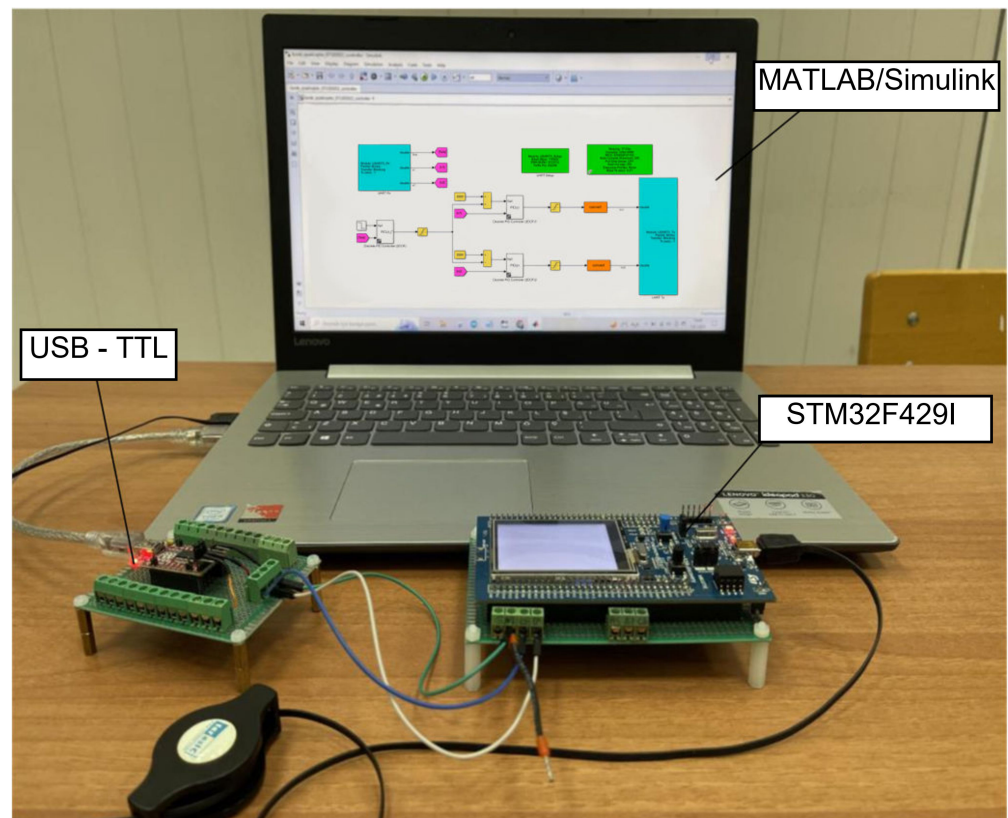


Figure 17. Simulation test setup created for the BLDCM driven 2R-UAV balance system.

In this study, classical and 2-DOF PID, and AF 2-DOF PID controller structures used to control the system were modeled using the Waijung Library in a Simulink environment. The created model was uploaded to the STM32F429I development board with a Build Model in Simulink. Subsequently, this environment was used to simulate the dynamic complete system, which was constructed utilizing the 2R-UAV balancing system model and the BLDCM and its drive system model. The Simulink model to be utilized in the Simulation, shown in Figure 18, was acquired by adding UART serial communication blocks to this developed model to connect with STM32F429I.

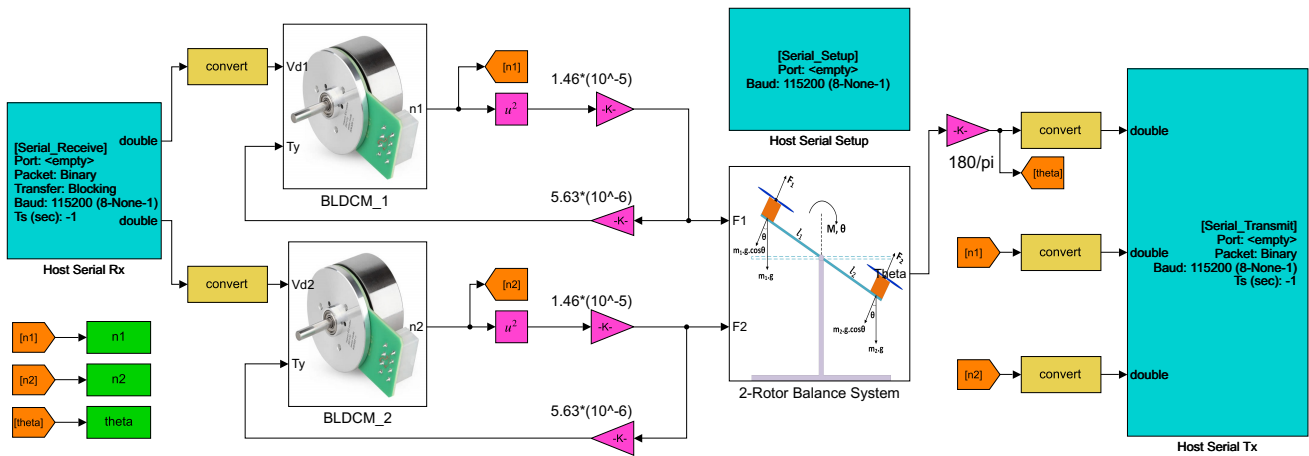


Figure 18. Matlab/Simulink Co-Simulation Model of BLDCM driven 2R-UAV balance system.

Figure 19 shows the classical and 2-DOF PID, and AF 2-DOF PID controller model, which was created using the Waijung library in the Simulink environment and loaded on the STM32F429I microprocessor for the control of the BLDCM driven 2R-UAV balance system. In this model, the model of the microprocessor to be used and the “clock” settings are made via the “Target Setup” block. The balance angle (θ) of the system, the speed of the BLDCM-1 (n_1) and the speed of the BLDCM-2 (n_2) taken from the 2R-UAV Balance System model created in Simulink are sent to the STM32F429I microprocessor via USB-TTL via the “UART Rx” block. The controller outputs created on the STM32F429I microprocessor are sent to Matlab/Simulink with the “UART Tx” block.

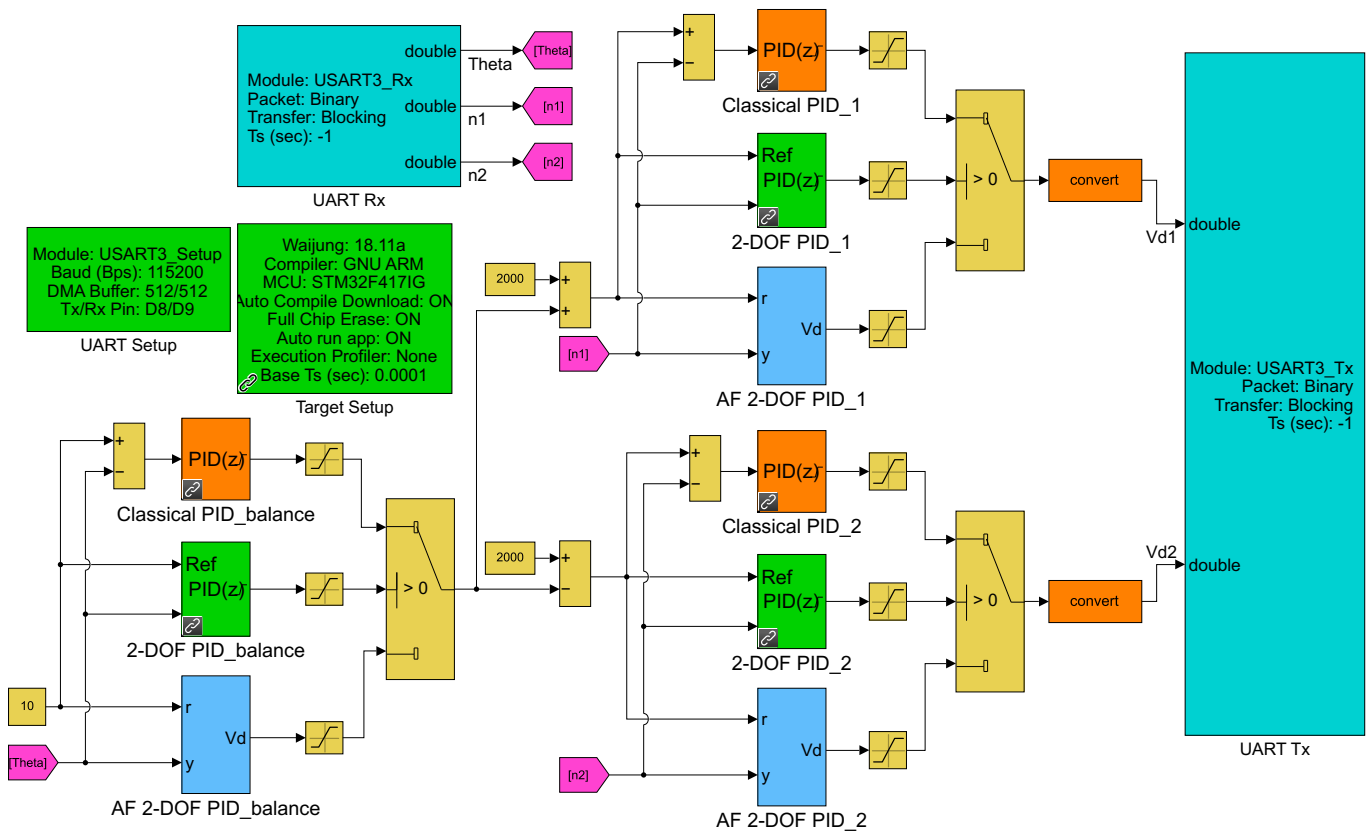


Figure 19. STM32F429I (STMMicroelectronics NV, Geneva, Switzerland) controller blocks created in Matlab/Simulink environment.

5. Results and Discussion

In the Co-Simulation studies, the system was controlled with the classical PID, 2-DOF PID, and AF 2-DOF PID controller. In order to analyse the controller performances, the system was tested with varying loads and reference values. In the first scenario, the reference balance angle is given as 10 degrees. In this case, the balance angle changes for all controllers given in Figure 20. Table 8 gives the performance criteria of the controllers for this scenario. As seen in Figure 20 and Table 8, all of the controllers caught the reference value in a short time and followed the reference steadily. However, although the 2-DOF PID controller achieved the reference earlier, the AF 2-DOF PID controller showed a finer performance than other controllers due to its lower overshoot value and less ripple value in steady state.

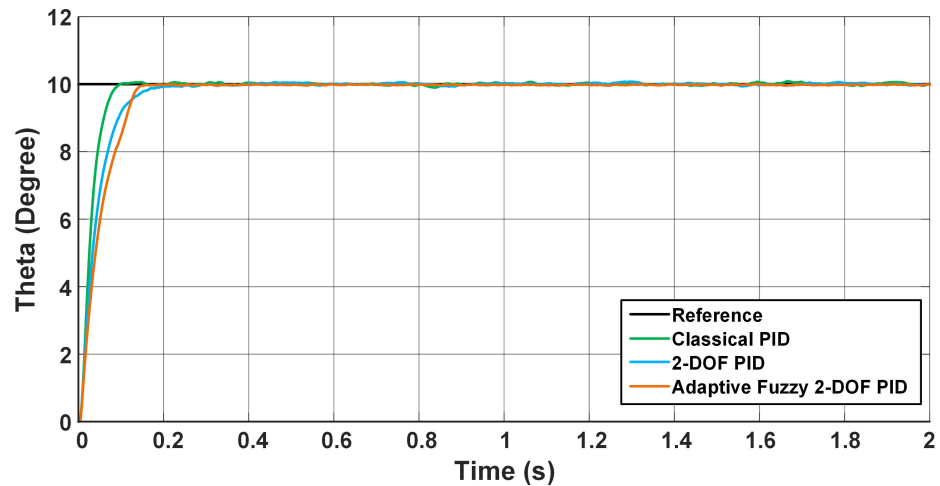


Figure 20. Changes on balance angle for 10 degrees reference.

Table 8. 2R-UAV Balance System controller comparisons by performance criteria.

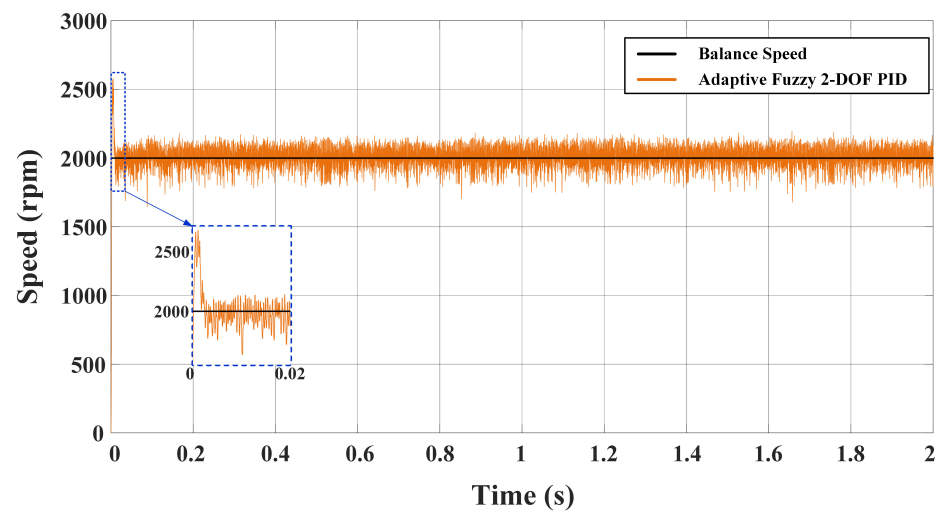
	Reference (Degree)	Performance Criteria	Classical PID Controller	2-DOF PID Controller	AF 2-DOF PID Controller
1. Scenario	0 to 10	Rising Time (s)	0.0496	0.0301	0.0605
		Settling Time (s)	0.0817	0.0536	0.0808
		Overshoot (%)	0.8372	1.0363	0
		Steady State Error	0.055	0.06	0.02
2. Scenario	0 to 30	Rising Time (s)	0.0529	0.0339	0.0619
		Settling Time (s)	0.0984	0.0590	0.0867
		Overshoot (%)	0.2392	0.7373	0
		Steady State Error	0.06	0.07	0.05
	30 to -30	Rising Time (s)	0.0471	0.0199	0.0283
		Settling Time (s)	0.1097	0.1120	0.0772
		Overshoot (%)	0.3139	5.6182	0
		Steady State Error	0.05	0.25	0.06

Figure 21 shows the speed change of both motors in the case with AF 2-DOF PID controller for the first scenario. When these speed changes are examined, it is seen that the speed of the BLDCM-1 increases and the speed of the BLDCM-2 decreases to ensure the 10 degree reference balance angle. Then, it is seen that both motors operate stably at an equilibrium speed of 2000 rpm.

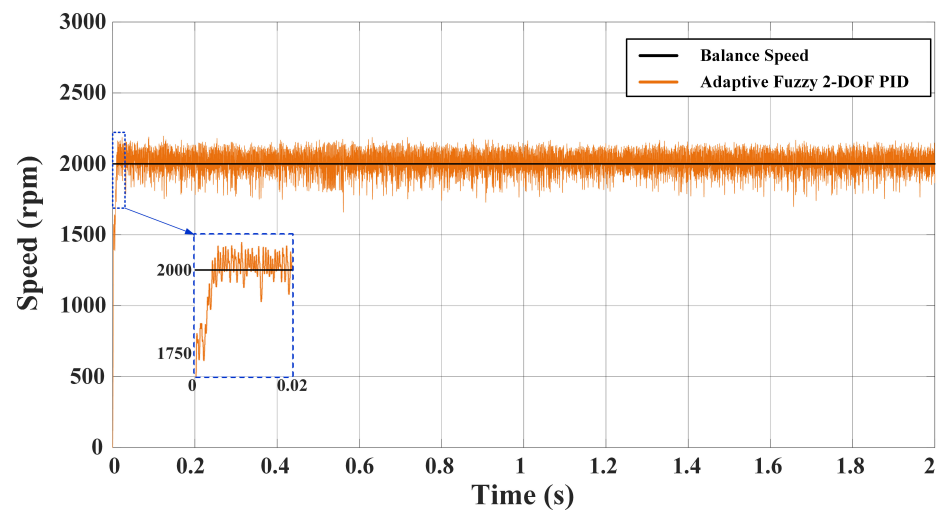
In the second scenario, the reference value of the balance angle is given as 30 degrees for a second and -30 degrees after the first second. In this case, the change of balance angle for all controllers is given in Figure 22. As seen in Figure 22, all of the controllers reached the reference value in a short time and followed the reference steadily. When the controller performance values given in Table 8 and Figure 22 are examined, the 2-DOF PID controller

reached the settled reference in a shorter time than the other controllers while the system went to the 30 degree reference balance angle. However, as the reference balance angle goes from 30 degrees to -30 degrees, it is seen that the AF 2-DOF PID controller proposed in this study has a shorter settling time than other controllers with the effect of adaptivity, and its overshoot and steady-state error are less.

Figure 23 shows the speed change of both motors in the case with AF 2-DOF PID controller for the second scenario. When these motor speed changes are examined, it is seen that the speed of the BLDCM-1 increases and the speed of the BLDCM-2 decreases to ensure the 30 degree reference balance angle at the start. When the reference position is reached, it is seen that both motors operate stably at 2000 rpm, which is the equilibrium speed. When the reference balance angle is reduced to -30 degrees, the speed of the BLDCM-1 decreases while the speed of the BLDCM-2 increases. Then, after the speed of both motors fluctuates for a short time, when the reference balance angle is reached, the motors operate stably at the balance speed.



(a) BLDCM-1



(b) BLDCM-2

Figure 21. Changes in motor speeds for 10 degrees balance angle reference.

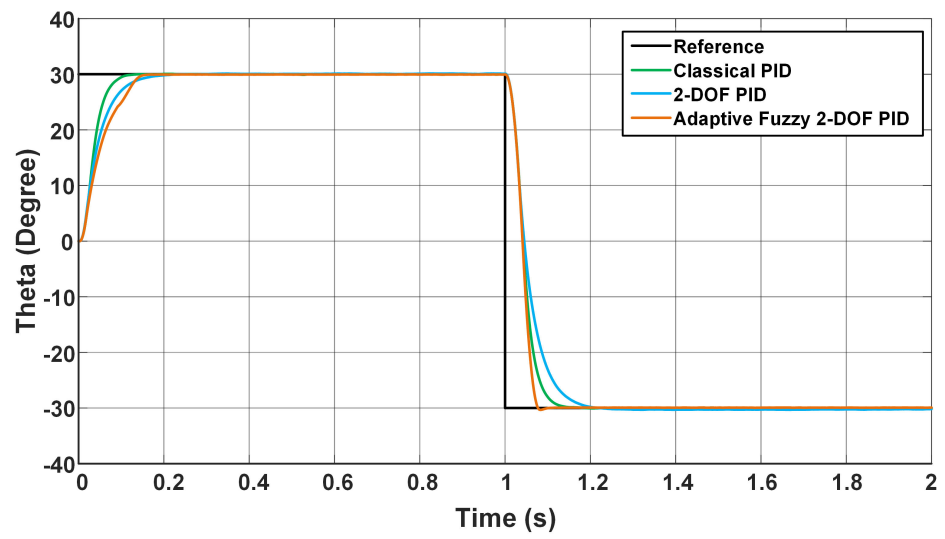
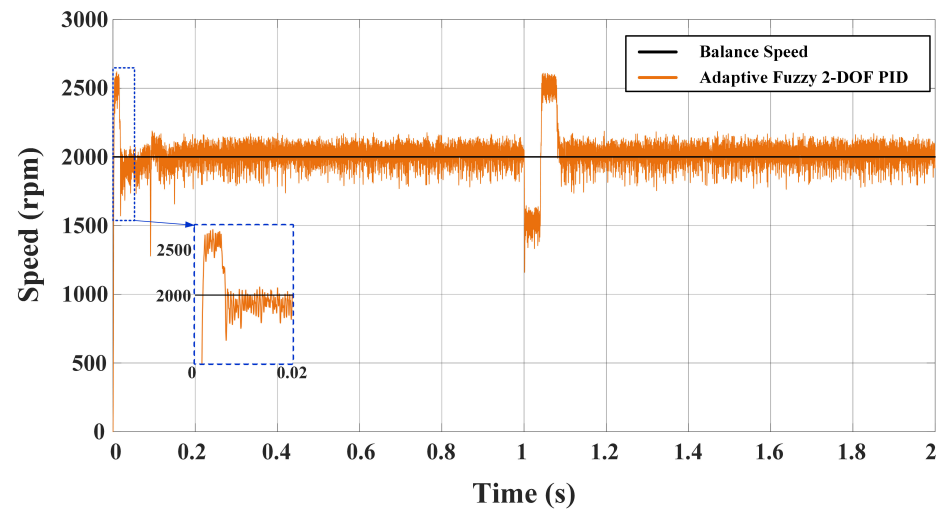
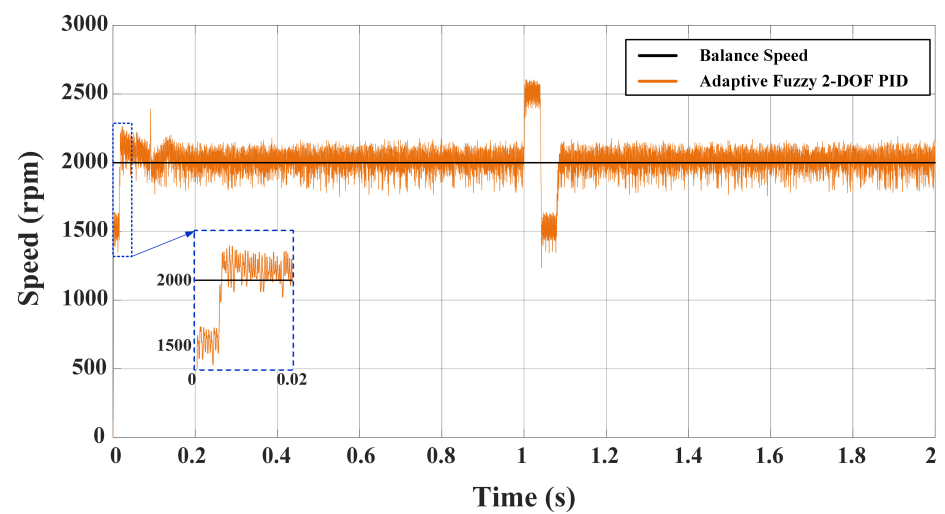


Figure 22. Changes in balance angle for 30 to -30 reference.



(a) BLDCM-1



(b) BLDCM-2

Figure 23. Changes in motor speeds for 30 to -30 degrees balance angle reference.

In order to examine the effect of the load on the controller performances in the 2R-UAV Balance System, in the third scenario, the reference balance angle was given as 10 degrees and after the first second, 250 g of load was added to the arm where the BLDCM-1 is located in the system, 15 cm away from the center. In this case, the change of balance angle for all controllers is given in Figure 24. When Figure 24 is examined, all controllers achieved the 10 degree reference balance angle in a short time, as given in the first scenario, and continued to operate stably. When the load was added in the first second, there was a short-term decrease in the balance angle for all controllers and then the reference balance angle was regained. However, it was observed that the AF 2-DOF PID controller proposed in this study achieved the reference balance angle with a much smaller decrease than other controllers.

Figure 25 shows both motor speeds for the third scenario with the AF 2-DOF PID controller. When these speed changes are examined, it is seen that there is no significant change in motor speeds when a load is added and both motors operate stably at 2000 rpm balance speed.

When the results obtained for all three scenarios are examined, it is seen that all the controllers used for balance angle and motor speed control in the BLDCM driven 2R-UAV balance system in this study successfully control the balance angle and motor speeds. However, we observed that the AF 2-DOF PID controller proposed in this study is more successful, especially under variable operating conditions, due to its adaptive feature.

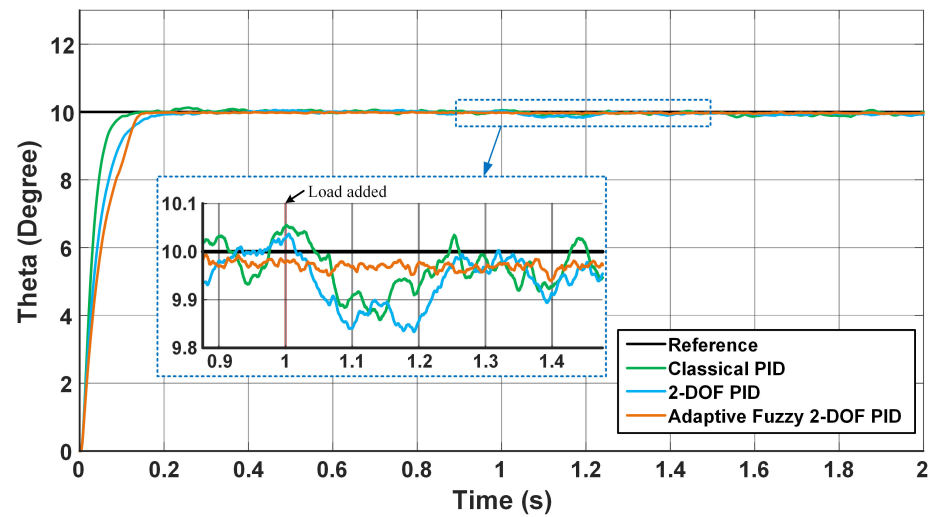
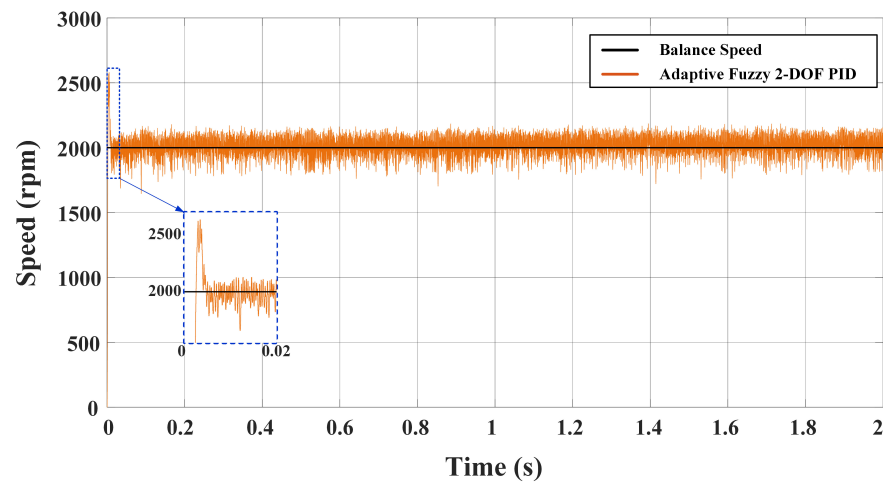
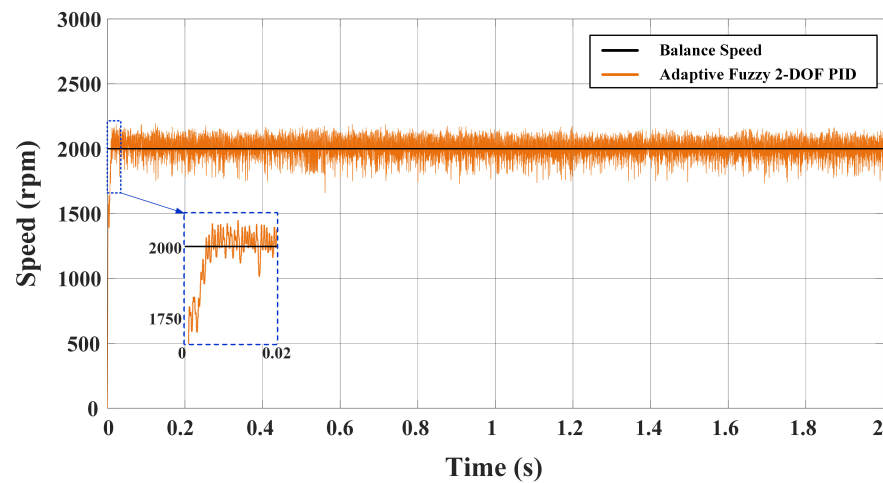


Figure 24. Changes of balance angle when condition of adding load.



(a) BLDCM-1



(b) BLDCM-2

Figure 25. Changes on motor speeds when condition of adding load.

6. Conclusions

Since the control and structure of multi-rotor systems in UAVs are much more complex than those of two-rotor systems, two-rotor systems are widely used in the literature to develop controllers. In this study, the stability control of a 2R-UAV with BLDCM as the drive element was performed. Differing from the studies in the literature, the speeds of the BLDCMs as well as the balance angle were controlled in a closed loop, improving the control performance of the balance angle. The controllers used were the PID controller, a classical control method; the 2-DOF PID controller, an advanced control method; and the AF 2-DOF PID controller, which combines Fuzzy Logic, an artificial intelligence-based control method, with the 2-DOF PID controller. To examine the real-time performance of the proposed controller structure, a Co-Simulation structure was created using an STM32F429I microprocessor and Matlab/Simulink simulations, and the results were examined.

Co-simulation results for the classical PID, advanced 2-DOF PID, and suggested AF 2-DOF PID controllers used for the control of the 2R-UAV Balance System are presented separately for fixed and variable reference balance angles, and loaded conditions. Examining these results, the reference balance angle was achieved in a short time in all operating situations and continued to operate stably. Nonetheless, it is evident that, particularly with changeable reference values and under load, the AF 2-DOF PID controller suggested in this work, thanks to its adaptive characteristics, performs better than both the PID and 2-DOF PID controllers. As seen in Table 8, the AF 2-DOF PID has 0% overshoot and the

minimum steady state error in all scenarios. Also, as seen in Figure 24, when the load was added, although there were no significant changes in the AF 2-DOF PID controlled system, a 0.1-degree drop occurred in the classical PID controlled system and a 0.15-degree drop in the 2-DOF PID controlled system.

The BLDCM driven 2R-UAV balance system modeled and controlled in this study is open to development in terms of its structure and suitable for the application of different control algorithms. In further studies, Artificial Neural Networks (ANN) and Deep Learning-based controller structures, which are artificial intelligence methods, will be tried for the control of the 2R-UAV Balance System. In addition, in this study, the AF 2-DOF PID controller structure, which is recommended for the control of 2R-UAV and shows successful performance, will be used to increase the control performance of the quad-rotor UAV, which is widely used today.

Author Contributions: Conceptualization, T.Y., H.C. and I.C.; methodology, H.C. and I.C.; software, H.C. and I.C.; validation, T.Y., H.C. and I.C.; formal analysis, I.C.; investigation, I.C.; resources, I.C.; data curation, I.C.; writing—original draft preparation, T.Y., H.C. and I.C.; writing—review and editing, T.Y. and H.C.; visualization, T.Y.; supervision, H.C.; project administration, H.C.; funding acquisition, H.C. and I.C. All authors have read and agreed to the published version of the manuscript.

Funding: This work has been supported within project MF21.75 by Firat University Scientific Research Projects Unit.

Data Availability Statement: The raw data supporting the conclusions of this article will be made available by the Author on request.

Conflicts of Interest: The Author declare that they have no known competing financial interests or personal relationships that could have appeared to influence the work reported in this paper.

Abbreviations

The following abbreviations are used in this manuscript:

BLDCM	Brushless Direct Current Motor
DOF	Degree of Freedom
PID	Proportional Integral Derivative Controller
UAV	Unmanned Aerial Vehicle
rpm	Revolutions per Minute

References

- Belge, E.; Hızır, K.; Parlak, A.; Altan, A.; Hacıoğlu, R. Estimation of small unmanned aerial vehicle lateral dynamic model with system identification approaches. *Balk. J. Electr. Comput. Eng.* **2020**, *8*, 121–126. [[CrossRef](#)]
- Cukdar, I.; Yigit, T.; Celik, H. BLDC Motor Driven, PSO Optimized 2-DOF PID Control of the Seesaw Balance System. In Proceedings of the 2021 13th International Conference on Electrical and Electronics Engineering (ELECO), Bursa, Turkey, 25–27 November 2021; IEEE: Piscataway, NJ, USA, 2021; pp. 114–118.
- Ali, Z.A.; Wang, D.; Aamir, M. Fuzzy-based hybrid control algorithm for the stabilization of a tri-rotor UAV. *Sensors* **2016**, *16*, 652. [[CrossRef](#)] [[PubMed](#)]
- Harun-Or-Rashid, M.; Wahid, N.B. Seesaw dynamics and control-experimental study. *J. Mech. Robot.* **2019**, *4*, 1–7.
- Kim, J.N.; Roh, M.S.; Song, J.B.; Song, W.J.; Kang, B.S.; Kim, J. An Experimental Study of a Single Axis Seesaw Attitude Control Consisting of Motor and Propeller. *J. Adv. Navig. Technol.* **2012**, *16*, 1–7. [[CrossRef](#)]
- Jayadi, A.; Adhinata, F.D.; Sembiring, J.P.; Putri, N.U.; Pranita, E.; Setiawan, A. Implementation of PID Control as a One Axis Balancing Control System on the Bicopter Vehicle. In Proceedings of the 2023 International Conference on Converging Technology in Electrical and Information Engineering (ICCTEIE), Bandar Lampung, Indonesia, 25–26 October 2023; IEEE: Piscataway, NJ, USA, 2023; pp. 113–117.
- Phillips, P.; Hrishikeshavan, V.; Rand, O.; Chopra, I. Design and development of a scaled quadrotor biplane with variable pitch propellers for rapid payload delivery. In Proceedings of the American Helicopter Society 72nd Annual Forum, West Palm Beach, FL, USA, 17–19 May 2016; pp. 17–19.
- Tashakori, A.; Ektesabi, M.; Hosseinzadeh, N. Modeling of BLDC motor with ideal back-EMF for automotive applications. In Proceedings of the World Congress on Engineering, San Francisco, CA, USA, 19–21 October 2011; Volume 2, pp. 6–8.
- Kroičs, K.; Būmanis, A. BLDC Motor Speed Control with Digital Adaptive PID-Fuzzy Controller and Reduced Harmonic Content. *Energies* **2024**, *17*, 1311. [[CrossRef](#)]

10. Yüzgeç, U.; Ökten, İ.; Üçgün, H.; Gün, A.R.; Türkyilmaz, T.; Kesler, M.; Karakuzu, C.; Gökhan, U. Development of the test platform for rotary wing unmanned air vehicle. *Bilecik Seyh Edebali Univ. J. Sci.* **2016**, *3*, 18–24.
11. Can, K.; Orman, K.; Başçı, A.; Derdiyok, A. Trajectory tracking control of a four rotor unmanned aerial vehicle (UAV) using two degree of freedom PI controller. In Proceedings of the 2016 National Conference on Electrical, Electronics and Biomedical Engineering (ELECO), Bursa, Turkey, 1–3 December 2016; IEEE: Piscataway, NJ, USA, 2016; pp. 682–686.
12. Eltayeb, A.; Rahmat, M.F.; Eltoun, M.M.; Ibrahim, M.S.; Basri, M.A.M. Trajectory tracking for the quadcopter uav utilizing fuzzy PID control approach. In Proceedings of the 2020 International Conference on Computer, Control, Electrical, and Electronics Engineering (ICCEEE), Khartoum, Sudan, 26 February–1 March 2021; IEEE: Piscataway, NJ, USA, 2021; pp. 1–6.
13. Rabah, M.; Rohan, A.; Han, Y.J.; Kim, S.H. Design of fuzzy-PID controller for quadcopter trajectory-tracking. *Int. J. Fuzzy Log. Intell. Syst.* **2018**, *18*, 204–213. [[CrossRef](#)]
14. Inayathullaah, M.; Sivakumar, N.; Balasundaram, A.; Arul, R.; Angalaeswari, S. Time Domain Investigation of Hybrid Intelligent Controllers Fed Five-Phase PMBLDC Motor Drive. *Appl. Sci.* **2023**, *13*, 3281. [[CrossRef](#)]
15. Celik, H.; Yigit, T. Field-oriented control of the PMSM with 2-DOF PI controller tuned by using PSO. In Proceedings of the 2018 International Conference on Artificial Intelligence and Data Processing (IDAP), Malatya, Turkey, 28–30 September 2018; IEEE: Piscataway, NJ, USA, 2018; pp. 1–4.
16. Özdemir, M.T. A novel optimum PI controller design based on stability boundary locussupported particle swarm optimization in AVR system. *Turk. J. Electr. Eng. Comput. Sci.* **2021**, *29*, 291–309. [[CrossRef](#)]
17. Mohammed, A.; Saidon, W.S.; Razak, M.A.A.; Samat, A.A.A. Optimization of PI Parameters for Speed Controller of a Permanent Magnet Synchronous Motor by using Particle Swarm Optimization Technique. *Int. J. Simul. Syst. Sci. Technol.* **2016**, *17*.
18. Zhang, Z.; Li, Y. An AEFA-Based optimum design of fuzzy PID controller for attitude control flywheel with BLDC motor. *Aerospace* **2022**, *9*, 789. [[CrossRef](#)]
19. Zhang, R.; Gao, L. The Brushless DC motor control system Based on neural network fuzzy PID control of power electronics technology. *Optik* **2022**, *271*, 169879. [[CrossRef](#)]
20. Ezzaldeen, M.M. Design of speed-controller for brushless dc-motor based on grey predictor-PID controller. *Eng. Technol. J.* **2018**, *36*, 900–905. [[CrossRef](#)]
21. Cunkas, M.; Aydoğdu, O. Realization of fuzzy logic controlled brushless dc motor drives using Matlab/Simulink. *Math. Comput. Appl.* **2010**, *15*, 218–229. [[CrossRef](#)]
22. Uurtsaikh, L.; Tengis, T.; Batmunkh, A. Control of Seesaw balancing using decision boundary based on classification method. *Int. J. Internet Broadcast. Commun.* **2019**, *11*, 11–18.
23. Usha, S.; Dubey, P.M.; Ramya, R.; Suganyadevi, M. Performance enhancement of BLDC motor using PID controller. *Int. J. Power Electron. Drive Syst.* **2021**, *12*, 1335. [[CrossRef](#)]
24. Preitl, S.; Stănean, A.I.; Precup, R.E.; Preitl, Z.; Petriu, E.M.; Dragoş, C.A.; Rădac, M.B. Controller design methods for driving systems based on extensions of symmetrical optimum method with DC and BLDC Motor Applications. *IFAC Proc. Vol.* **2012**, *45*, 264–269. [[CrossRef](#)]
25. Couceiro, M.; Ghamisi, P.; Couceiro, M.; Ghamisi, P. *Particle Swarm Optimization*; Springer: Berlin/Heidelberg, Germany, 2016.
26. Bunday, B.D.; Kiri, V.A. Maximum likelihood estimation—Practical merits of variable metric optimisation methods. *J. R. Stat. Soc. Ser. Stat.* **1987**, *36*, 349–355. [[CrossRef](#)]
27. Kennedy, J.; Eberhart, R. Particle swarm optimization. In Proceedings of ICNN'95—International Conference on Neural Networks, Perth, WA, Australia, 27 November–1 December 1995; IEEE: Piscataway, NJ, USA, 1995; Volume 4, pp. 1942–1948.
28. Huseyin Bilgic, H.; Conker, C.; Yavuz, H. Fuzzy logic-based decision support system for selection of optimum input shaping techniques in point-to-point motion systems. *Proc. Inst. Mech. Eng. Part I J. Syst. Control Eng.* **2021**, *235*, 795–808. [[CrossRef](#)]
29. Yıldız, S.; Gunduz, H.; Yildirim, B.; Özdemir, M.T. An innovative LFC scheme for multi-area microgrid incorporating with hydrogen-based demand response mechanism. *Int. J. Hydrogen Energy* **2023**, *48*, 39425–39441. [[CrossRef](#)]
30. Çelebi, M. Genetic Algorithm Based Optimal Adaptive Fuzzy PID Controller Synthesis. Master's Thesis, Yildiz Technical University, Istanbul, Turkey, 2011.
31. Asadi, F.; Pongswatd, S. *Programming the ARM® Cortex®-M4-based STM32F4 Microcontrollers with Simulink®*; Morgan & Claypool Publishers: San Rafael, CA, USA, 2021.

Disclaimer/Publisher's Note: The statements, opinions and data contained in all publications are solely those of the individual author(s) and contributor(s) and not of MDPI and/or the editor(s). MDPI and/or the editor(s) disclaim responsibility for any injury to people or property resulting from any ideas, methods, instructions or products referred to in the content.